Spectroscopy of the transition state: Elementary reactions of the hydroxyl radical studied by photoelectron spectroscopy of $O^-(H_2O)$ and $H_3O_2^-$

Don W. Arnold,[a] Cangshan Xu, and Daniel M. Neumark[b]
Department of Chemistry, University of California, Berkeley, California 94720 and Chemical Sciences Division, Lawrence Berkeley Laboratory, Berkeley, California 94720

(Received 7 November 1994; accepted 11 January 1995)

The transition state regions of the $OH+OH\rightarrow O(^3P)+H_2O$ and the $OH+H_2O\rightarrow H_2O+OH$ reactions are studied by photoelectron spectroscopy of the $O^-(H_2O)$ and $H_3O_2^-$ anions and their deuterated analogs. The spectra show resolved vibrational progressions attributed to H-atom vibrational motion in the unstable neutral complexes formed by photodetachment. The positions and intensities of the peaks change markedly upon isotopic substitution. One-dimensional Franck–Condon calculations using *ab initio* potentials for the anion and neutral are used to interpret the peak spacings and intensities, as well as the strong isotopic effects. The results are discussed in the context of previously obtained transition state spectra for heavy+light–heavy reactions. © *1995 American Institute of Physics.*

I. INTRODUCTION

In recent years, negative ion photoelectron spectroscopy has been demonstrated to provide a powerful and detailed probe of the transition state region in bimolecular chemical reactions.[1] In these experiments, the transition state region is accessed by photodetachment of a stable negative ion with a geometry similar to that of the neutral transition state; the resulting photoelectron spectrum probes the spectroscopy and dissociation dynamics of the transition region species. Several reactions have been studied with this method, including heavy–light–heavy hydrogen transfer reactions ($X+HY\rightarrow XH+Y$; X,Y=I,Br,Cl,F),[2,3] hydrogen abstraction reactions by fluorine ($OH+F\rightarrow O+HF$ and $ROH+F\rightarrow RO+HF$; R=CH_3O, C_2H_5O),[4] and the prototypical $F+H_2$ reaction.[5] In this article, we present the results of recent experiments in our laboratory where the photoelectron spectra of the $H_3O_2^-$ and $O^-(H_2O)$ anions are collected to study the unstable neutral complexes involved in two fundamental reactions of the hydroxyl radical

$$OH+H_2O\rightarrow H_2O+OH, \tag{1}$$

$$OH+OH\rightarrow O(^3P)+H_2O. \tag{2}$$

The role of the hydroxyl radical as a propagator of chain reactions makes it extremely important in atmospheric chemistry, combustion chemistry, and a wide range of other chemically active environments.[6] The hydroxyl radical is known to play a vital role in the stratospheric ozone chemistry through the HO_x cycle.[7] It also acts to remove many chemical species which are important in tropospheric chemistry, including CO, H_2S, SO_2, and CH_3CCl_3.[8] The reaction of $O(^1D)+H_2O$ serves as a major source of tropospheric OH radicals.[9] In combustion, reaction (2) and its reverse reaction serve as termination and propagation steps, respectively, in the oxidation of hydrogen.[10]

This set of experiments studying the transition state species of hydroxyl radical reactions not only begins our study of this extremely important class of bimolecular reactions but also continues the extension of our transition state studies to reactions with polyatomic reactants and\or products. Both of the reactions studied here represent quite fundamental chemical reactions that are accessible to accurate study by *ab initio* methods. To date, however, only a few detailed theoretical studies exist for either reaction (1) or (2).

Figures 1 and 2 show schematic energy diagrams for reactions (1) and (2). Since the anion geometry and energetics play a key role in our experiment, the energetics for the analogous ion–molecule reactions are also shown. The figures represent the energy of the systems as a function of generic reaction coordinates. In Fig. 1, both the anion and neutral reactions are thermoneutral due to symmetry. The $H_3O_2^-$ anion is calculated to have a single minimum (see Sec. III B),[11] and its dissociation energy, $D_0(OH^-\cdots H_2O)=1.18$ eV, has been measured by high pressure mass spectrometry.[12] The electron affinity of OH [EA(OH)=1.825 eV][13] has been accurately measured by threshold photodetachment of OH^-. The values shown for the neutral potential curve are from *ab initio* calculations. Schaefer and co-workers[14] calculated van der Waals minima of 0.15 eV (3.5 kcal/mole) for the $OH(H_2O)$ complex in the hydrogen-bonded configuration which is applicable to the photodetachment experiments. The global minimum was found to occur in a different intramolecular configuration which is not conducive to hydrogen exchange and lies 0.13 eV (3.1 kcal/mole)[15] lower in energy than the local minimum shown in Fig. 1. A barrier height of 0.56 eV (13 kcal/mole) for the reaction was determined in an *ab initio* investigation by Nanayakkara *et al.*[16]

In Fig. 2, the shape of the anion potential is adapted from Lifshiftz[17] and is based upon an anion reaction model developed by Brauman and co-workers.[18] However, no actual characterization of this anion potential surface has been made (i.e., the height of the barrier between the two geometries, if one exists, has not been determined). Limits for the binding energies of the $O^-(H_2O)$ and $OH^-(OH)$ anions have been determined by flow tube kinetics[19,20] and pulsed high

[a]Current Address: Department of Chemistry, University of Southern California, Los Angeles, CA 90089.
[b]Camille and Henry Dreyfus Teacher–Scholar.

 0021-9606/95/102(15)/6088/12/$6.00 © 1995 American Institute of Physics
Downloaded 03 Mar 2005 to 128.32.220.130. Redistribution subject to AIP license or copyright, see http://ojps.aip.org/jcpo/jcpcr.jsp

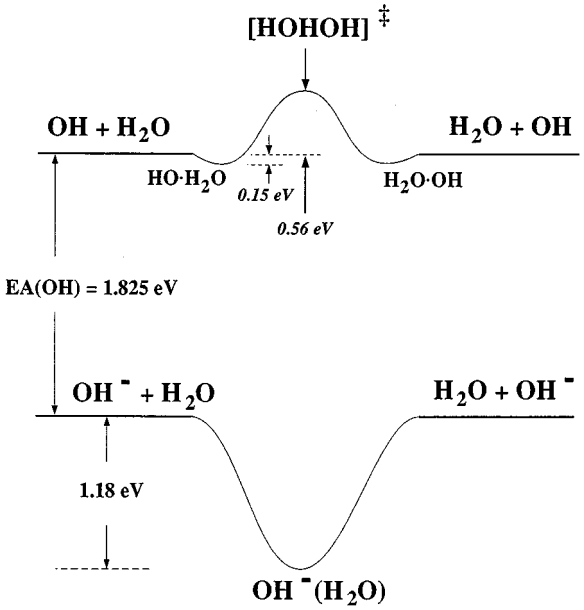

FIG. 1. Schematic energetics diagram for the $H_3O_2^-/OH+H_2O$ system. Values in italics are theoretically determined values. References given in text.

pressure mass spectrometry.[21] Note that these experimental limits do not indicate whether there are two geometries corresponding to local minima in the potential energy surface separated by a barrier or if the two structures are actually indistinguishable. The electron affinity of oxygen has also been measured by anion threshold photodetachment.[22] Similarly to $OH+H_2O$, a van der Waals minimum is also predicted to exist on the OH+OH triplet surface. Fueno[23] predicts the dipole–dipole complex to be bound by 6.9 kcal/mole. However, Harding suggests that the binding energy is more on the order of 4.2 kcal/mole.[24] Harding and Wagner calculate a 2.3 kcal/mole barrier for the reaction.[25]

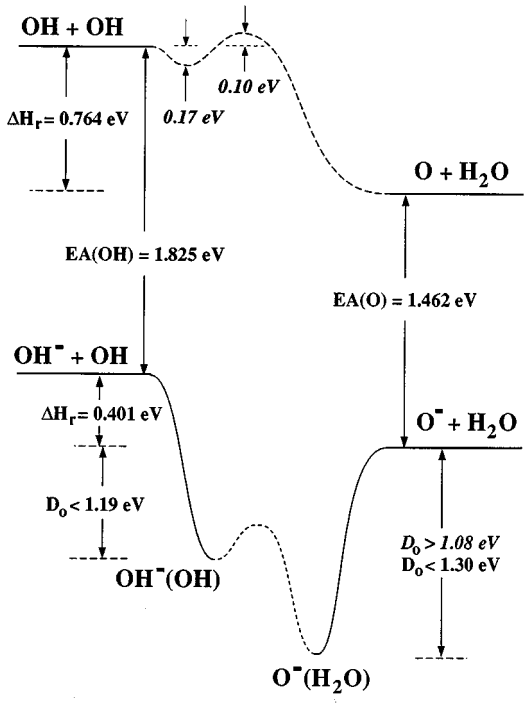

FIG. 2. Schematic energetics diagram for the $O^-(H_2O)/OH+OH$ system. Values in italics are theoretically determined values. References given in text.

Photodetachment of the $H_3O_2^-$ anion was first studied by Golub and Steiner over 25 years ago.[26] The total photodetachment cross section was measured as a function of photon energy up to 4 eV. The monotonic increase observed in their photoelectron signal with increasing photon energy beyond 2.8 eV was interpreted as photodetachment of the $OH^-(H_2O)$ anion cluster to form a dissociative neutral complex. No underlying structure was resolved in the data obtained from their early study. Since then, however, the $H_3O_2^-$ anion has been characterized by x-ray structural analysis after its observation in the crystals of transition metal complexes.[27] This anion has also been observed in the IR spectra of tetraalkylammonium ion hydroxide hydrate complexes.[28] The photoelectron spectra of $H_3O_2^-$ presented below show resolved features which contain information about the dynamics near the transition state region of reaction (1). The $OH+H_2O$ reaction has been studied using oxygen atom isotopic exchange measurements. The gas phase reaction rate constant was determined[29] to be $<1\times10^{-15}\,cm^3\,molecule^{-1}\,s^{-1}$ at 298 and 373 K. The rate of reaction (1) in solution, initiated by pulsed radiolysis, has also been investigated in conjunction with a study of the $O^-+H_2O\rightarrow OH^-+OH$ reaction.[30]

Reaction (2) has been more thoroughly investigated experimentally. Numerous measurements of the rate of reaction (2) over various temperature ranges[31–40] show that hydroxyl radical disproportionation has a non-Arhennius behavior.[41] Measurements for the rate of the reverse reaction have also been made and found to be consistent with these findings.[42] The source of this non-Arhennius behavior has been debated with respect to the presence or absence of a potential barrier along the reaction path. Initially, Wagner and Zellner[32] suggested a barrierless reaction in which the long-range attractive forces affected the temperature dependence of the reaction. Harding and Wagner have since calculated a 2.3 kcal/mole barrier and conclude that the long range forces do not play a major role in the reaction's temperature dependence.[25] Recent results by Michael[43] are consistent with the results of Ref. 25. While the O^-+H_2O reaction has been studied by several groups[44–49] and $O^-(H_2O)$ has been observed by mass spectrometry in $H_2/O_2/N_2$ flames,[50] no experimental characterization of the $O^-(H_2O)$ anion has been completed which can confirm the results of the *ab initio* calculations to be presented in Sec. III B.

The reverse of reaction (2) may also play a role in experiments studying $O(^1D)+H_2O\rightarrow OH+OH$ where O atoms are generated by ozone photolysis.[51,52] Sauder *et al.*[52] estimate that as much as 10% of the observed OH products may result from reactions of $O(^3P)$ ground state atoms with the water molecules in these photoinitiated reaction experiments.

In the following sections, we will briefly describe the experiments performed (Sec. II) and present the results obtained (Sec. III A). *Ab initio* calculations to be used in the

Downloaded¬03¬Mar¬2003¬to¬128.32.220.150. Redistribution¬subject¬to¬AIP¬license¬or¬copyright,¬see¬http://ojps.aip.org/jcpo/jcpcr.jsp

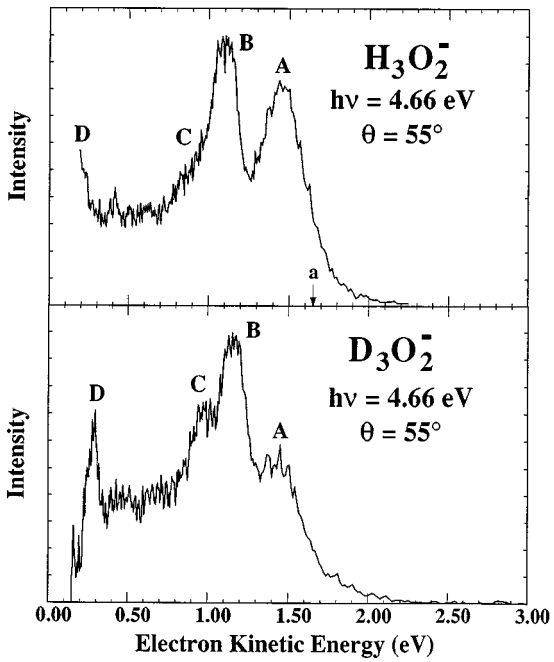

FIG. 3. Photoelectron spectra of $H_3O_2^-$ and $D_3O_2^-$ collected using a 4.657 eV photodetachment energy. The arrow *"a"* indicates the asymptotic energy for the $OH+H_2O$ ground state products.

analysis of the data are described in Sec. III B. The results of these calculations are used in one-dimensional Franck–Condon analyses to qualitatively understand the photoelectron spectra in terms of the dynamics in the transition state region of the reaction. Comparisons will be drawn with our studies of related fluorine atom reactions (OH+F and CH_3OH+F) which we have investigated previously.[4]

II. EXPERIMENT

The apparatus employed in these experiments, described in detail previously,[3] is a dual time-of-flight anion photoelectron spectrometer. Details relevant to the present results will be summarized here. Anions of interest are generated in the source region at the intersection of a pulsed molecular beam and a 1 keV electron beam, using a configuration similar to that developed by Johnson *et al.*[53] A gas mixture (4% H_2O or D_2O, 96% N_2O), at a stagnation pressure of 1 bar, is expanded through the molecular beam valve orifice (0.020 in.) at a repetition rate of 20 Hz. The 1 keV electron beam intersects the molecular beam at the orifice of the molecular beam valve. At this intersection, a variety of chemical processes occur which lead to the formation of $O^-(H_2O)$ and $H_3O_2^-$ anions. O^- anions, generated by dissociative attachment of low-energy electrons to N_2O,[54,55] can form $O^-(H_2O)$ by termolecular clustering reactions or OH^- by $O^-+H_2O \rightarrow OH^-+OH$. Hydroxide ions which are generated can also cluster to H_2O molecules to form the $H_3O_2^-$ clusters. As shown by Melton[56] and others, electron bombardment of H_2O generates H^-, O^-, and OH^- anions, all of which can contribute to ion formation. As the expansion continues, the molecules relax rotationally and vibrationally by collisions with the carrier gas.

The cooled ions are extracted into a Wiley–McLaren-type time-of-flight mass spectrometer[57] where the ions separate, according to mass, from other anions which are formed in the source region. The mass resolution of the apparatus, $M/\Delta M \sim 250$, allows easy separation of the $H_3O_2^-$ and $O^-(H_2O)$ ions. The ion of interest is then selectively photodetached by a properly timed 8 ns Nd:YAG laser pulse. Photoelectrons, detected with 70 mm multichannel plates, are energy analyzed after time-of-flight measurements through a 1 m field-free flight tube oriented perpendicular to the mass spectrometer flight tube. The resolution of the apparatus is 8 meV for electrons with 0.65 eV of electron kinetic energy (eKE) and degrades as $(eKE)^{3/2}$. For these experiments, the fourth harmonic (266 nm; 15 mJ/pulse) of the Nd:YAG laser was employed for photodetachment. The plane-polarized laser beam can be rotated with a half-wave plate in order to study photoelectron angular distributions.

III. RESULTS

A. Experimental results

Figure 3 shows the photoelectron spectra collected for $H_3O_2^-$ and $D_3O_2^-$. Figure 4 displays the $O^-(H_2O)$ and $O^-(D_2O)$ spectra. In these spectra, the relationship between the eKE and the internal energy of the neutral complex is given by

$$\mathrm{eKE} = h\nu - D_0 - \mathrm{EA} - E_{\mathrm{int}}^0 + E_{\mathrm{int}}^-. \tag{3}$$

In Eq. (3), D_0 is the lowest dissociation energy of the anion complex [i.e., $D_0(OH^-\cdots H_2O)$ or $D_0(O^-\cdots H_2O)$ given in

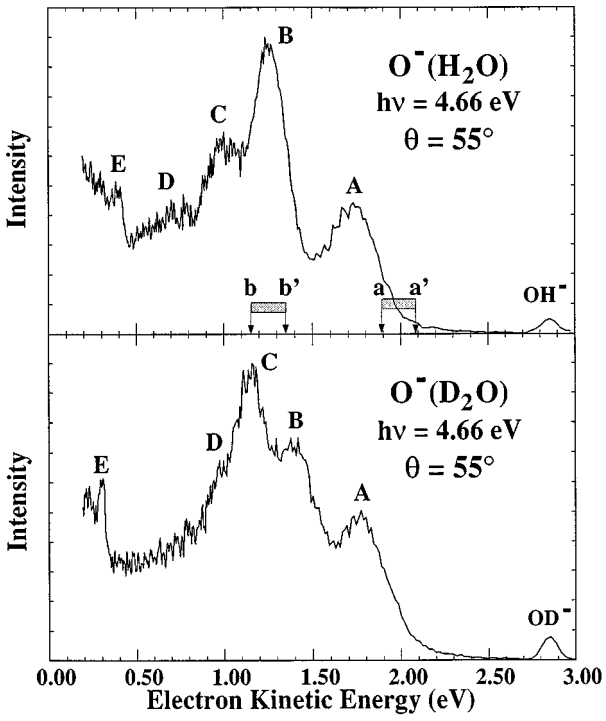

FIG. 4. Photoelectron spectra of $O^-(H_2O)$ and $O^-(D_2O)$ collected using a 4.657 eV photodetachment energy. The regions a/a' and b/b' indicate the limits for the asymptotic energies for dissociation of the neutral complex into $O+H_2O$ and OH+OH, respectively.

Downloaded¬03¬Mar¬2003¬to¬128.32.220.150. Redistribution¬subject¬to¬AIP¬license¬or¬copyright,¬see¬http://ojps.aip.org/jcpo/jcpcr.jsp

TABLE I. Peak positions and widths for the $H_3O_2^-$ and $D_3O_2^-$ 4.66 eV photoelectron spectra.[a]

Peak	eKE (eV)	Energy (cm^{-1})	Width (eV)
$H_3O_2^-$			
A	1.45	0.0	0.33
B	1.10	2823	0.19
C	0.91	4355	0.21
$D_3O_2^-$			
A	1.45	0.0	0.33
B	1.16	2339	0.20
C	0.94	4113	0.21
D	0.293[b]	···	···

[a]Position of peak center and full width at half-maximum (FWHM) as determined by fit to a Gaussian-shaped peak. No consideration is made for superimposed vibrational structure.
[b]Intensity severely affected by electron detector cutoff function.

TABLE II. Peak positions and widths for the $O^-(H_2O)$ and $O^-(D_2O)$ 4.66 eV photoelectron spectra.[a]

Peak	eKE (eV)	Energy (cm^{-1})	Width (eV)
$O^-(H_2O)$			
A	1.72	0.0	0.34
B	1.27	3629	0.22
C	1.00	5807	0.27
D	~0.7	~8200	0.3
E	0.40[b]	10646	···
$O^-(D_2O)$			
A	1.76	0.0	0.34
B	1.41	2823	0.25
C	1.15	4920	0.22
D	0.925	6734	0.21
E	0.297[b]	11800	···

[a]Position of peak center and full width at half-maximum (FWHM) as determined by fit to a Gaussian-shaped peak. No consideration is made for superimposed vibrational structure.
[b]Intensity severely affected by electron detector cutoff function.

Figs. 1 and 2] and EA is the electron affinity of the fragment anion [i.e., EA(OH)=1.825 eV (Ref. 13) and EA(O)=1.462 eV (Ref. 22)]. $E_{\rm int}^-$ and $E_{\rm int}^0$ represent the internal energies of the anion and neutral complexes, respectively. For the anion, $E_{\rm int}^-$ is the internal energy above the zero point. For the neutral [HOHOH] complex, $E_{\rm int}^0$ is the energy above the separated $OH+H_2O$ ground state fragments. For the [HOHO] complex, $E_{\rm int}^0$ is the energy above the ground state $O+H_2O$ products.

In each of the spectra, the energetic asymptotes for dissociation of the neutral complex are indicated by arrows; features at lower eKE than the arrows correspond to neutral states with sufficient energy to dissociate. In Fig. 3, the arrow marked "*a*" indicates the $OH+H_2O$ limit while in Fig. 4 the regions bounded by the a/a' and b/b' arrows indicate the limits for the $O+H_2O$ (product) and OH+OH (reactant) ground state energetic asymptotes; the large uncertainties reflect the uncertainty in $D_0(O^-–H_2O)$. Clearly, almost all of the signal in the spectra is from neutral states which can dissociate into either reactants or products.

There are several similarities between the $H_3O_2^-$ and the $O^-(H_2O)$ spectra. The spectra consist primarily of very broad, irregularly spaced features. Isotopic substitution significantly changes not only the positions of the features but also the intensities. The centers, widths, and spacings of the broad features in the $H_3O_2^-$ and $D_3O_2^-$ spectra are given in Table I. Those for the $O^-(H_2O)$ and $O^-(D_2O)$ spectra are given in Table II. Based upon previous studies of the heavy–light–heavy hydrogen exchange reactions,[2,3] we expect these features to be related to the antisymmetric stretch motion of the "transfer" hydrogen atom between the oxygen atoms (i.e., $O\cdots\overleftrightarrow{H}\cdots O$).

Another common feature to the data sets is the appearance of a feature at very low eKE. The intensity of this feature (labeled as *D* in the $H_3O_2^-$ spectra and *E* in the $O^-(H_2O)$ spectra) is suppressed by the electron detector cutoff function. The large energy separation from the other features in the spectrum suggests that the low eKE feature represents photodetachment to electronically excited neutral complexes. Another piece of evidence which supports this assignment is the change in position of peak *E* upon isotopic substitution. As seen in Fig. 4, peak *E* moves to *lower* eKE upon deuteration. This effect is consistent with the assignment of this feature to an excited state which undergoes a smaller zero point energy decrease than the anion upon deuteration.

Also seen in the $O^-(H_2O)$ and $O^-(D_2O)$ photoelectron spectra is a feature near 2.85 eV. This peak occurs at the same energy as signal for OH^- photodetachment. We believe that this feature corresponds to a sequential two-photon process. The $O^-(H_2O)$ anion is photodissociated into OH^-+OH followed by photodetachment of the OH^- anion during the same 8 ns laser pulse, as demonstrated previously by Buntine *et al.*[49] A less intense signal was also observed at ~3.2 eV which corresponds to O^- photodetachment after photodissociation of $O^-(H_2O)$ into O^-+H_2O.

B. *Ab initio* calculations

As an aid to the interpretation of the data presented above, we have performed *ab initio* calculations using the Gaussian92 package for the anion and neutral complexes involved in these experiments. The calculations include geometry optimizations and potential energy curve calculations along selected coordinates. While not intended as state-of-the-art calculations for these systems, the results are to be used in simple model calculations to understand, qualitatively, the features observed in the photoelectron spectra. We are specifically interested in the anion and neutral potentials along the $O\cdots H\cdots O$ hydrogen transfer coordinate.

1. Anion calculations

Several studies of the hydrogen bonding characteristics of the closed-shell $H_3O_2^-$ ion have been carried out previously using *ab initio* methods.[11,58,59] However, in most of these studies, only partial geometry optimizations were performed with one or more fixed parameters. The full optimization by Rohlfing *et al.*[11] at the MP2/6-31G** level of theory resulted in a complex with a linear, symmetric $O\cdots H\cdots O$ arrangement within a nonplanar overall $H_3O_2^-$ geometry as shown in Fig. 5. From these results, it appears that

Downloaded¬03¬Mar¬2003¬to¬128.32.220.150. Redistribution¬subject¬to¬AIP¬license¬or¬copyright,¬see¬http://ojps.aip.org/jcpo/jcpcr.jsp

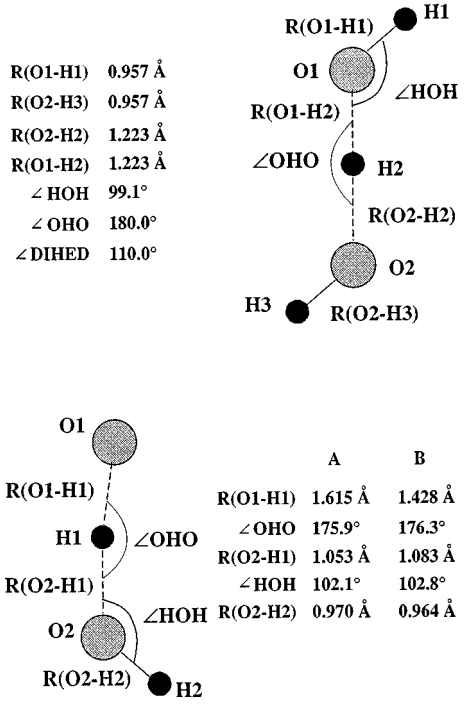

FIG. 5. *Ab initio* calculated geometries for the $H_3O_2^-$ and $O^-(H_2O)$ anions. Values for $H_3O_2^-$ are from Ref. 11. For $O^-(H_2O)$, values "*A*" are MP2/6-31+G* parameters from Ref. 60 and values "*B*" are MP2/6-31++G** parameters determined in the present study. See text for details.

the strong hydrogen bond which exists in the $H_3O_2^-$ anion leads to a rather short O–O distance (~2.4 Å) with the hydrogen atom centered between the two oxygen atoms. No further optimizations of the $H_3O_2^-$ geometry are pursued here.

As seen in Fig. 5, the dihedral angle of $H_3O_2^-$ is calculated to be 110°. Since the hindered rotation/torsional motion is expected to be somewhat floppy, we have calculated the MP2/6-31++G** energy of the complex as a function of the dihedral angle with all of the other geometrical parameters fixed. The shape of the potential curve and the height of the "*trans*" barrier (~120 cm^{-1} at π radians), shown in Fig. 6, agrees with Spirko *et al.*'s[59] calculations using different fixed parameters, but the "*cis*" barrier (~600 cm^{-1} at 0 radians) is significantly larger than that obtained by Spirko (~300 cm^{-1}). In their analysis, they find a zero point energy of 62 cm^{-1} for the hindered rotor motion. Thus, while the potential minima occur at dihedral angles of 110° and 250°, the anion torsional motion is very floppy with an average dihedral angle of 180°.

With this in mind, potential energy curves for the antisymmetric O···H···O motion of *trans*-$H_3O_2^-$ are calculated at the MP2/6-31++G** level of theory using a dihedral angle of 180° (the "*trans*" configuration). In addition to the dihedral angle, several other parameters are frozen to calculate the potential for this coordinate (see caption for Fig. 7). The central hydrogen atom, H2, was allowed to move between two oxygen atoms which were fixed at R(O1–O2)=2.4 Å. The resultant potential energy curve (Fig. 7, bottom) has a very flat bottom with a minimum which occurs at the centrosymmetric nuclear configuration.

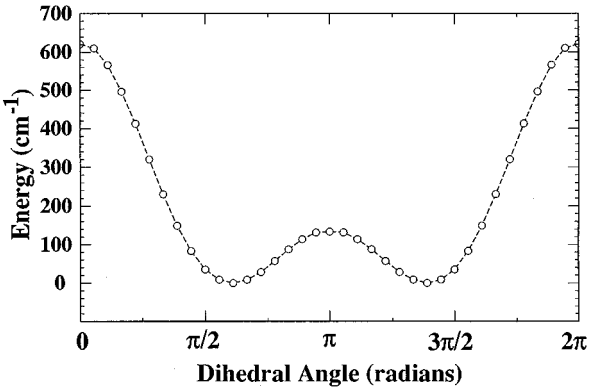

FIG. 6. *Ab initio* potential energy curve for the $H_3O_2^-$ hindered rotor motion at the MP2/6-31++G** level of theory. The dihedral angle is varied while the other geometrical parameters are fixed as R(O1–O2)=2.4 Å; R(O1–H1) $=R$(O2–H3)=0.962 Å; R(O1–H2)=R(O2–H2)=1.2 Å; OHO=180°; HOH =104.5°.

Fewer theoretical studies of the $O^-(H_2O)$ anion have been made as a result of the more complicated open-shell interaction. Roehl *et al.*[60] find that the $O^-(H_2O)$ anion is most stable in a planar, "quasilinear" configuration (Fig. 5) at the MP2/6-31+G* level of theory. The geometry of this quasilinear species is reoptimized here at the MP2/6-31++G** level of theory to include additional basis functions on the hydrogen atoms. The optimized parameters from both calculations are summarized in Fig. 5. In all of the calculations, the OHO angle is nearly linear while the HOH angle is slightly more acute than the angle found in H_2O. The extended R(O2–H1) bond length as compared to R(O2–H2) indicates that considerable hydrogen bonding occurs be-

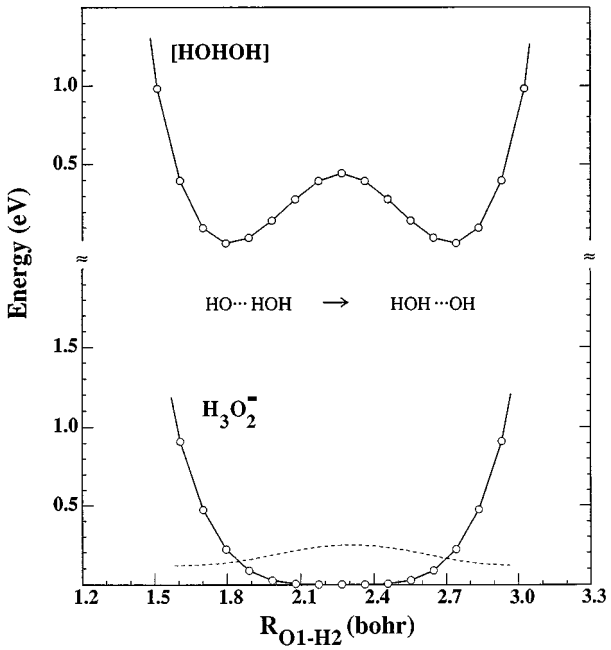

FIG. 7. *Ab initio* calculated potential energy curves for $H_3O_2^-$ and HOHOH along the central hydrogen atom antisymmetric stretch coordinate. The H-atom position is varied while the other parameters are fixed as R(O1–O2) =2.4 Å; R(O1–H1)=R(O2–H3)=0.962 Å; OHO=180°; HOH=99.1°; dihedral=180°.

Downloaded¬03¬Mar¬2003¬to¬128.32.220.150. Redistribution¬subject¬to¬AIP¬license¬or¬copyright,¬see¬http://ojps.aip.org/jcpo/jcpcr.jsp

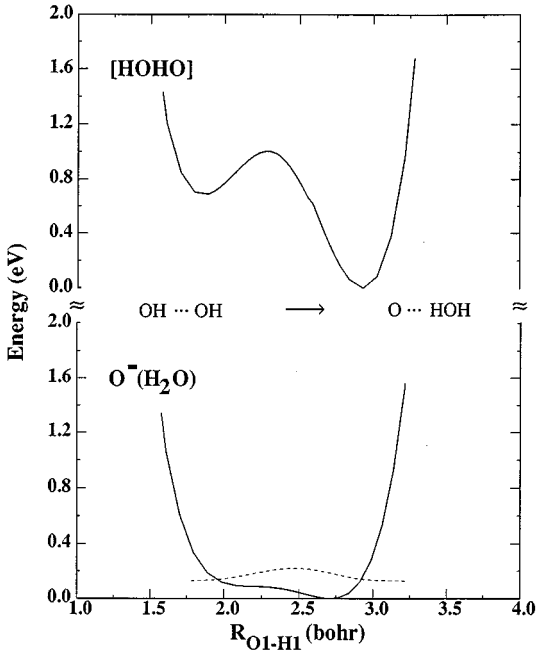

FIG. 8. *Ab initio* calculated potential energy curves for $O^-(H_2O)$ and HOHO along the central H-atom antisymmetric stretch vibrational coordinate. The H-atom position is varied while the other geometrical parameters are fixed as R(O1–O2)=2.5 Å; R(O2–H3)=0.962 Å; OHO=180°; HOH =102.8°.

tween the O^- and the H_2O but not as much as in the $H_3O_2^-$ anion. The calculated anion ground state has $^2A''$ symmetry, with the unpaired electron in an orbital perpendicular to the plane of symmetry.

The antisymmetric O···H···O motion of $O^-(H_2O)$ is also investigated as in the case of $H_3O_2^-$. In this case, the potential energy curves are calculated at the QCISD/6-31++G** level of theory. As for the $H_3O_2^-$ calculations, several parameters are fixed. While the OHO bond angle is assumed to be linear for simplicity, the remainder of the frozen parameters are based upon the *ab initio* results and are given in caption for Fig. 8. Along the constrained O···H···O coordinate, the potential energy curve for the ground electronic state (Fig. 8, bottom) has a single minimum which occurs at the equilibrium geometry. However, there is a shelf in the potential, corresponding to the OH^-–OH geometry, which is <0.1 eV above the minimum in the curve. Note that this does not mean there is no $OH^-\cdot OH$ local minimum; such a minimum could occur at a different O–O distance than the one considered here.

2. Neutral calculations

We have also calculated potential energy curves for the neutral $[HOHOH]^‡$ and $[HOHO]^‡$ complexes along the O···H···O coordinate. These will be used in the Franck–Condon simulations presented in the following section. In these calculations, which are performed at the same levels of theory used for the anions, the coordinates other than the O···H···O coordinate are fixed at the same values used in the anion calculations. The calculated curves, shown in Figs. 7 and 8, respectively, represent one-dimensional ''slices'' through the $O+H_2O$ and $OH+H_2O$ reaction surfaces. (See Figure 6 in Ref. 2a to see how such a slice is taken through a two-dimensional potential energy surface.) Both curves show double minima. Note that these do not correspond to minima of the neutral surfaces but rather to points where the 1-D slice through the reaction surfaces intersects the bottom of the reactant and product valleys. Also, the barriers in the 1-D curves do not directly relate to the barrier along the minimum energy reaction path but are instead the barrier separating the reactant and product valleys at a given O–O separation.

The minima in the 1-D potential functions for $[HOHOH]^‡$ in Fig. 7 correspond to geometries of the complex with C_s symmetry, and the molecular orbitals for both the anion and neutral will be labeled using this point group. Thus, the $H_3O_2^-$ anion has a $(\cdots(6a')^2(7a')^2(1a'')^2(8a')^2(2a'')^2)$ orbital occupation at the MP2/6-31++G** level of theory; the $8a'$ and $2a''$ orbitals have σ_u and π_g symmetry, respectively, with respect to the O–H–O bond. Photodetachment of the anion can lead to either a $^2A'$ or a $^2A''$ state, both of which correlate to the ground state $OH+H_2O$ dissociation products of the neutral $[HOHOH]^‡$ complex. The surface shown in Fig. 7 is the $^2A'$ surface which is calculated to be lowest in energy at the MP2/6-31++G** level of theory in the Franck–Condon region. At the minimum energy anion geometry used in the potential curve calculations, the $^2A'$ state is predicted to lie $\sim$0.58 eV below the $^2A''$ state at the MP2/6-31++G** level of theory.[61] The barrier to symmetric hydrogen exchange along this restricted O···H···O coordinate is 0.50 eV at the MP2/6-31++G** level of theory.

For OH+OH, the interaction of two ground state hydroxyl radicals splits the $OH(^2\Pi)$ states into four singlet states and four triplet states. The hydroxyl radical disproportionation, reaction (2), can occur adiabatically on three of the four triplet states along a C_s planar reaction path.[32] Based upon the orbital occupation calculated for the $O^-(H_2O)$ anion, $(\cdots(6a')^2(1a'')^2(7a')^2(8a')^2(2a'')^1)$, one-electron photodetachment from either of the two highest molecular orbitals can form the $^1A'$, $^1A''$, or $^3A''$ species. Of these possibilities, the lowest energy species at the geometry of the anion is the $^3A''$ state; the corresponding surface is the one on which the OH+OH reaction is most likely to produce $O(^3P)+H_2O$.[23,24] A $^3A'$ state is calculated to lie $\sim$2.4 kcal/mole[24] above the $^3A''$ state at the saddle point but since this electronic state has unpaired electrons in two different a' orbitals $[\cdots(7a')^1(8a')^1(2a'')^2]$ it is not accessible by one-electron photodetachment of the $O^-(H_2O)$ anion. Therefore, we have calculated the potential energy curve for the $^3A''$ state along the constrained O···H···O coordinate; the result is shown in Fig. 8. The two minima are separated by 0.690 eV, and the barrier height is 0.322 eV with respect to the OH–OH minimum.

Two hydroxyl radicals can also react to form H_2O_2; the singlet surface on which this reaction occurs correlates to $O(^1D)+H_2O$.[62] The $O^-(H_2O)$ anion clearly has very poor Franck–Condon overlap with H_2O_2, so our experiment does not probe the region of the surface near the H_2O_2 well. How-

Downloaded¬03¬Mar¬2003¬to¬128.32.220.150. Redistribution¬subject¬to¬AIP¬license¬or¬copyright,¬see¬http://ojps.aip.org/jcpo/jcpcr.jsp

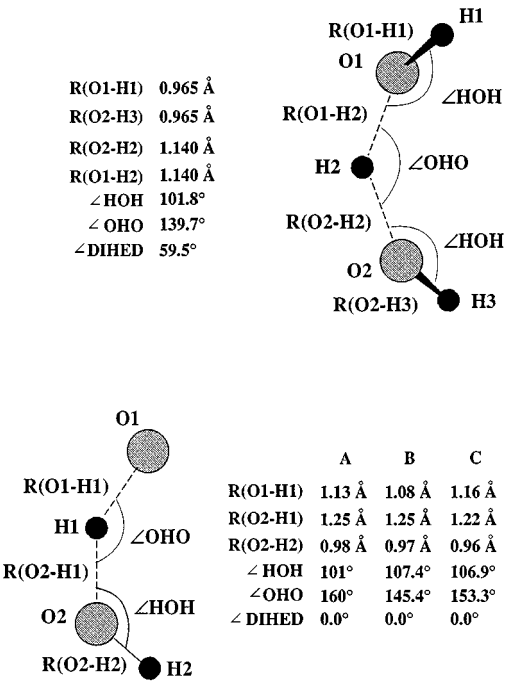

FIG. 9. *Ab initio* calculated transition state geometries for the $OH+H_2O \rightarrow H_2O+OH$ and $OH+OH \rightarrow O+H_2O$ reactions. Parameters for $[HOHOH]^{\ddagger}$ are from Ref. 16. For $[HOHO]^{\ddagger}$, "*A*" parameters are UHF/4-31G values from Ref. 23, "*B*" parameters are MCSCF/DZP values from Ref. 25, and "*C*" parameters are MP2/6-31++G** values are from the present work. See text for details.

ever, peak *E* in the $O^-(H_2O)$ photoelectron spectrum may be due to a transition to this surface near the product $O(^1D)+H_2O$ asymptote.

It is also of interest to calculate the transition state geometries (i.e., saddle point geometries) for the two neutral reactions. The transition state structure of the $OH+H_2O$ reaction has been investigated in detail by Nanayakkara *et al.*[16] Their best calculated transition state geometry (Fig. 9) lies on a barrier estimated to be 0.46 eV above the separated products. No further investigation is made of this species. For the OH+OH reaction, the $^3A''$ saddle point species has been located previously at the self-consistent field (SCF)[23] and multiconfiguration SCF (MCSCF)[24] level of theory. We have located the stationary point at the MP2/6-31++G** and QCISD/6-31++G** levels of theory. The geometries for the $[HOHO]^{\ddagger}$ structure calculated at these various levels of theory are given in Fig. 9.

IV. ANALYSIS AND DISCUSSION

A. Initial considerations

The appearance of each photoelectron spectrum is primarily determined by the Franck–Condon (FC) overlap between the bound anion ground state wave function and the scattering wave functions on the $OH+HX \rightarrow X+H_2O$ (X =OH,O) reaction surfaces. Thus, the success of negative ion photoelectron spectroscopy as a probe of reaction dynamics in the transition state region is contingent upon having significant Franck–Condon overlap between the anion ground state and the transition state region of the neutral reaction surface. It is therefore useful to compare the calculated geometries for the anions and neutral transition state species.

Both of the anions used in this study have significant hydrogen bonding character. The calculated equilibrium geometries for these anion species (Fig. 5) indicate that the central hydrogen atom interacts significantly with both oxygen atoms. The very flat antisymmetric stretch potential for both anions (Fig. 7 and 8) results in an extended hydrogen atom motion and a large FC region for the photodetachment process. Based upon the classical turning points for the $v'=0$ level of the calculated one-dimensional potential curves, R(O1–H2) varies from 0.99 to 1.42 Å for $H_3O_2^-$, and R(O1–H1) varies from 1.06 to 1.56 Å for $O^-(H_2O)$.

A comparison of the anion equilibrium geometries (Fig. 5) to the calculated transition state structures (Fig. 9) finds reasonable overlap between the anion and neutral geometries. The O–O separation in the transition state species is shorter than that of the ion in both cases. The OHO bond angles are also slightly different, with the anions being more linear than the neutral transition state in both cases. Both types of deviation between anion and neutral transition state are similar to several of the XHX^- systems studied previously in this laboratory.[2,3] Overall, the FC region will be centered slightly away from the saddle point toward the entrance and exit channels, but it should still be in the transition state region for both reactions. This is supported by the vibrational structure in the spectra, discussed below.

To assess the relationship of the features observed in the photoelectron spectra to the dynamics which occur at the transition state of reactions (1) and (2), several factors must be considered. A good starting point is the general appearance of the data. All of the data consist of several very broad features [full width at half maximum (FWHM)~0.2 eV or greater] which are irregularly spaced in energy and which lie above the neutral dissociation asymptote. By forming the anions in a molecular beam expansion, we produce anions which are primarily in their ground vibrational state. Thus, the spacings observed between features in the photoelectron spectrum will be representative of the vibrational motions of the unstable neutral complex. These vibrations must correspond to motions which are approximately perpendicular to the reaction coordinate and have vibrational periods which are on a time scale shorter than that of the dissociation process. Otherwise, only a structureless spectrum would be observed. In the $OH+H_2O$ and OH+OH systems, the reaction coordinate is described, to a good approximation, by the O–O separation.

As mentioned in Sec. III A, the isotopic dependence shows that the vibrations primarily involve hydrogen atom motion. While the observed peak spacings are quite irregular, it is useful to compare them to the observed vibrational frequencies of the "component" OH ($\omega_e=3735$ cm^{-1})[63] and H_2O ($\nu_1=3657$ cm^{-1}; $\nu_2=1595$ cm^{-1}; $\nu_3=3756$ cm^{-1})[64] molecules. The observed *A*-*B* spacing in the $H_3O_2^-$ spectrum (~2800 cm^{-1}) does not match well with any of the "component" frequencies. The *B*-*C* spacing is significantly smaller (~1500 cm^{-1}). In the case of the $O^-(H_2O)$ data, the *A*-*B* spacing (~3600 cm^{-1}) is near the OH stretching frequencies of the OH radical and the H_2O molecule. However,

Downloaded¬03¬Mar¬2003¬to¬128.32.220.150. Redistribution¬subject¬to¬AIP¬license¬or¬copyright,¬see¬http://ojps.aip.org/jcpo/jcpcr.jsp

as for the $H_3O_2^-$ spectrum, the *B*-*C* spacing is significantly smaller ($\sim$2300 cm^{-1}) and does not match any of the ''component'' frequencies.

This substantial perturbation of vibrational frequencies relative to OH and H_2O indicates that the central hydrogen atom interacts significantly with both of the oxygen atoms in the neutral complexes. Thus these experiments are, in fact, probing the transition state region for reactions (1) and (2). The observed irregular energy level spacings are also consistent with the eigenvalue spectrum expected from the double minimum potentials calculated for the [HOHO] and [HOHOH] complexes; the relation between these potentials and the spectra will be considered more quantitatively in the next section.

The observed peak widths are at least an order of magnitude greater than the experimental resolution. This observation is similar to that observed in previous transition state spectra of heavy–light–heavy anions. These result from homogeneous contributions due to the lifetime of the neutral complex, and from inhomogeneous contributions due to unresolved progressions in low frequency vibrational modes of the complex. In some cases, it has been possible to resolve this finer vibrational structure. For example, progressions in the low frequency bend and symmetric stretch modes were seen in the IHI^- zero electron kinetic energy (ZEKE) spectrum,[65] and bend/hindered rotor progressions were observed in the FH_2^- photoelectron spectrum[5] and inferred in the recent analysis of the $OHCl^-$ photoelectron spectrum.[66] For the $O^-(H_2O)$ and $H_3O_2^-$ spectra, it is not immediately obvious whether lifetime effects or unresolved transitions are primarily responsible for the peak widths. However, based upon the calculated geometries for the anions and the neutral transition state species, we expect a significant amount of bend/hindered rotor excitation of the neutral upon anion photodetachment.

B. Franck–Condon simulations

To put the discussion in the previous section on more quantitative ground, it is useful to compare the data with a Franck–Condon simulation of the spectra. An exact simulation requires an accurate determination of the anion geometry, a high quality potential energy surface for the neutral reaction, and a complex scattering calculation. While these requirements have recently resulted in a successful simulation of the FH_2^- spectrum,[5] the systems presented here are insufficiently characterized to warrant such a treatment.

We have shown previously that analysis within a reduced dimensionality model can provide valuable and insightful information about the photoelectron spectra.[2–4] In heavy–light–heavy triatomic systems studied previously, simple treatments of the data employed one-dimensional (1-D) and two-dimensional (2-D) slices from semiempirical potential energy surfaces along coordinates which could possibly be active in the photoelectron spectrum. These simple analyses revealed quite clearly that the major features in the photoelectron spectra of other heavy–light–heavy systems could be assigned to the antisymmetric hydrogen atom motion in the neutral transition state complex. However, such semiempirical potential energy surfaces have not been constructed for reactions (1) and (2) yet. As an alternative approach, we will use the one-dimensional *ab initio* potential energy curves along the antisymmetric hydrogen stretch coordinate for the anion and neutral (Sec. III B). These potential energy curves can then be used to calculate one-dimensional stick spectra which may be compared to the data.

The polynomial functions determined from least-squares fit to the *ab initio* data points for both the anion and the neutral complexes are used to determine 1-D Franck–Condon factors (FCFs) along the approximate hydrogen atom antisymmetric stretch vibrational coordinate. In this model, both the anion and neutral potential functions support a set of bound quantum states such that, within the FC approximation, the intensity of a photodetachment transition is given by

$$I \propto v_e \cdot |\tau_e|^2 \cdot |\langle \psi_{v'}(Q_{\mathrm{as}}) | \psi_{v''}(Q_{\mathrm{as}}) \rangle|^2. \tag{4}$$

In Eq. (4), $\psi_{v''}$ and $\psi_{v'}$ are the vibrational wave functions of the anion and neutral, respectively, along the hydrogen atom antisymmetric stretch vibrational coordinate, Q_{as}, and v_e is the asymptotic velocity of the photodetached electron. In the simulations, the electronic transition dipole, τ_e, is assumed to be constant as a function of eKE. For each potential function, eigenvalues and eigenfunctions are determined numerically by standard matrix methods.[67] The eigenfunctions are used to determine the Franck–Condon factors by numerical integration. An appropriate change in the reduced mass allows calculation of FCF's for the deuterated analogs using the same potential energy curves. In the figures shown below, the stick spectra will be compared directly with the data. In addition, the stick spectra will be convoluted with the experimental resolution function plus an additional Gaussian with FWHM=200 meV for comparison to the broad features observed in the experimental data.

Shown in Fig. 10 are the results of the $H_3O_2^-$ and $D_3O_2^-$ simulations calculated by the above method using the anion and potential energy curves calculated at MP2/6-31++G** level of theory. The simulations are superimposed upon the experimental data for comparison of peak spacings, intensities, and isotope dependence. Since the simulations assume that all of the anions are in their ground vibrational state, the peaks spacings in the simulations are indicative of the energy levels which are supported by the neutral potential energy surfaces. Fixing the terminal OH bond lengths at equal values imposes a symmetry about the center of the potential energy curves. Due to this symmetry, only transitions to even states of the neutral have nonzero intensity. Thus, the features in the simulation represent photodetachment transitions to the $v'=0$, $v'=2$, and $v'=4$ vibrational states supported by the neutral potential energy curve. In both the $H_3O_2^-$ and $D_3O_2^-$ spectra, the observed peak spacings are reasonably well reproduced by the simulations. Although the intensity of peak *C* is underestimated in both simulations, the observed change in peak intensities that result from isotopic substitution is very well modeled. The positions of these peaks, their relative integrated intensities, and their assignments are given in Table III.

Downloaded¬03¬Mar¬2003¬to¬128.32.220.150. Redistribution¬subject¬to¬AIP¬license¬or¬copyright,¬see¬http://ojps.aip.org/jcpo/jcpcr.jsp

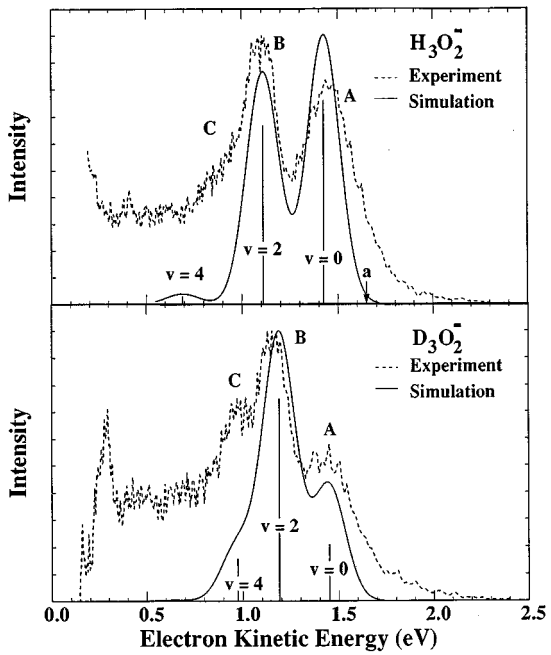

FIG. 10. Experimental data (dotted) and Franck–Condon simulations (solid) for $H_3O_2^-$ and $D_3O_2^-$. Franck–Condon factors are calculated using the *ab initio* surfaces shown in Fig. 7.

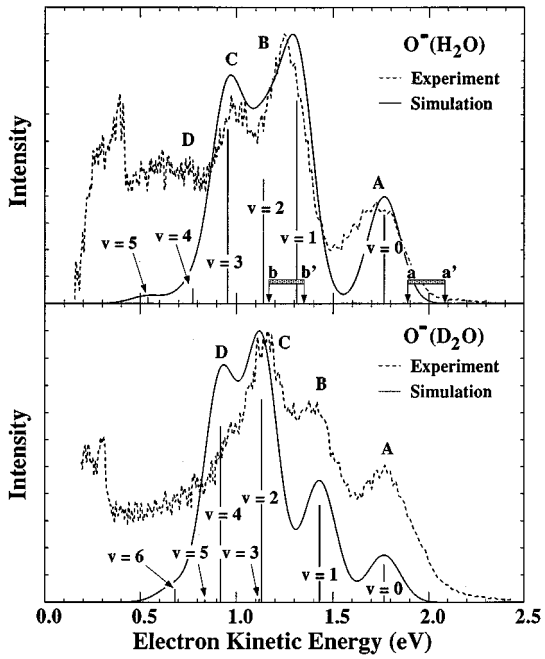

FIG. 11. Experimental data (dotted) and Franck–Condon simulations (solid) for $O^-(H_2O)$ and $O^-(D_2O)$. Franck–Condon factors are calculated using the *ab initio* surfaces shown in Fig. 8.

Shown in Fig. 11 are the results of the $O^-(H_2O)$ and $O^-(D_2O)$ simulations. In general, there is reasonable agreement between the convoluted 1-D simulations and the photoelectron spectra, particularly for the $O^-(H_2O)$ spectrum. Note that since there is no symmetry in these potentials, transitions to all of the neutral vibrational levels are allowed, as indicated. As might be expected, the peak positions change upon isotopic substitution. The peak shifts are not uniform, however. Inspection of the simulated peak positions given in Table IV shows that the $v'=1$ and the $v'=3$ transitions shift by 963 and 1315 cm^{-1}, respectively, to higher eKE while the $v'=2$ peak shifts 85 cm^{-1} to *lower* eKE. Although the length of the $O^-(D_2O)$ progression is overestimated, the simulations also reproduce the change of relative intensities upon isotopic substitution. However, the intensity pattern is very irregular. This is particularly true for the $O^-(D_2O)$ simulation where the $v'=2$ feature is the dominant transitions while $v'=3$ has almost no intensity. A similar situation occurs for the $v'=4/v'=5$ pair.

In order to understand the significant changes in peak spacings and intensities that occur upon isotopic substitution, it is useful to study the wave functions that are supported by the 1-D potential energy curves calculated for the restricted O···H···O motion of the neutral complexes. As shown in Fig. 7, the maximum in the $H_3O_2^-$ anion ground state wave function occurs at the location of the barrier in the symmetric neutral potential. In Fig. 12, the calculated neutral potentials for the $[HOHOH]^‡$ and $[DODOD]^‡$ complexes are shown again with their corresponding eigenvalues and eigenfunctions. For both complexes, the $v'=0$ and 1 levels lie below the barrier. Upon deuteration, the $v'=0$ level drops in energy and its amplitude in the region of the barrier is reduced. Hence, its overlap with the anion wave function is reduced, and the corresponding peak (peak *A*) in the photoelectron spectrum should be smaller in agreement with experiment. This effect has been observed previously in XHX^- photoelectron spectra.[1]

The $O^-(H_2O)$ anion ground state wave function (Fig. 8), while overlapping both the reactant and product wells, has its greatest amplitude at a geometry which corresponds to the

TABLE III. Simulated peak positions for the $H_3O_2^-$ and $D_3O_2^-$ spectra.

	H		D	
v'	Energy (cm^{-1})	Intensity	Energy (cm^{-1})	Intensity
0	0.0	1.0	0.0	0.28
1	125	0.0	49	0.0
2	2548	0.88	2105	1.0
3	3819	0.0	2489	0.0
4	5922	0.03	3842	0.21

TABLE IV. Simulated peak positions for the $O^-(H_2O)$ and $O^-(D_2O)$ spectra.

	H		D	
v'	Energy (cm^{-1})	Intensity	Energy (cm^{-1})	Intensity
0	0.0	0.44	0.0	0.18
1	3664	1.0	2701	0.48
2	5032	0.62	5117	1.0
3	6527	0.86	5212	0.02
4	7989	0.07	6814	0.87
5	9890	0.03	7480	0.01
6	···	···	8746	0.06

Downloaded¬03¬Mar¬2003¬to¬128.32.220.150. Redistribution¬subject¬to¬AIP¬license¬or¬copyright,¬see¬http://ojps.aip.org/jcpo/jcpcr.jsp

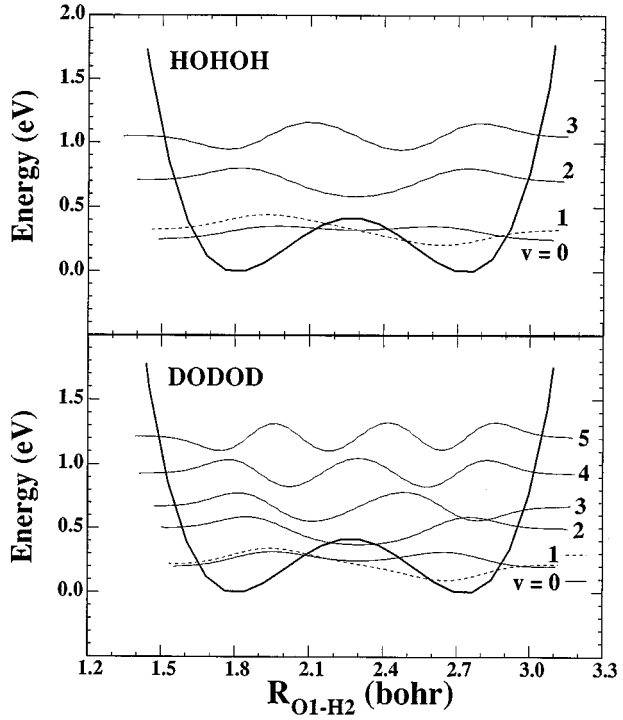

FIG. 12. The MP2/6-31++G** neutral potential energy curves for the HOHOH complex (as in Fig. 7) with the associated eigenfunctions and eigenvalues.

product side ($O+H_2O$) of the barrier. The terms ''reactant'' and ''product'' relate to the valleys in the multidimensional potential energy surface which correspond to the minima in the 1-D potential functions used in these calculations.

Shown in Fig. 13 are the neutral curves for HOHO and DODO with the associated eigenvalues and eigenfunctions. The effects of the barrier in this case are more interesting as a result of the asymmetry of the potential functions. The $v'=0$ and $v'=1$ levels are localized in the product well for both the hydrated and deuterated species. However, the $v'=2$ and $v'=3$ levels of HOHO are located near the barrier between the reactant and product wells. Upon isotopic substitution, we see that the $v'=2$ and $v'=3$ vibrational levels and the $v'=4$ and $v'=5$ levels of DODO form nearly degenerate pairs. Further inspection of the $v'=2/v'=3$ eigenfunction pair for DODO shows that one of the levels ($v=2$) is primarily localized in the product well while the other ($v=3$) has most of its intensity in the reactant well. Within each pair of DODO levels, the combination of different nodal structures and localization for the wave function results in markedly different FCFs for consecutive states (Table IV and Fig. 11). Thus the $v'=2$ state has good FC overlap with the anion function while that of the $v'=3$ level is nearly zero. A similar effect occurs for the $v'=4$ and $v'=5$ levels. For the HOHO complex, the intensity alternation between adjacent levels is less dramatic.

It is interesting to consider how the spectra relate to the asymptotic dynamics as a function of the vibrational ''level'' of the unstable neutral complex. The neutral that results from photodetachment of $H_3O_2^-$ has only one dissociation channel, $OH+H_2O$. However, the [HOHO] complex has two accessible dissociation channels at the photodetachment energy used. As indicated by the arrows a/a' and b/b' in Figs. 4 and 11 the $O+H_2O$ product channel is open to all of the observed vibrational levels, but the OH+OH reactant channel becomes accessible only at the higher vibrational levels. For example, peak *A* in both the $O^-(H_2O)$ and $O^-(D_2O)$ spectra is energetically limited to product dissociation, while peak *C* in both spectra can dissociate to both reactant and product. While peak *B* is limited to product dissociation in $O^-(D_2O)$, the uncertainty in the asymptote prevents an assignment for feature *B* in the $O^-(H_2O)$ spectrum.

The 1-D wave functions suggest reactant/product specificity beyond what is energetically allowed. For [DODO], the $v'=2$ and $v'=4$ states are localized in the product well, while the $v'=3$ and $v'=5$ states, which have poor FC overlap with the anion, are localized in the reactant well. Thus, within the limits of the wave functions of this 1-D model and their FC overlap with the anion, these results suggest that a DODO complex generated from $O^-(D_2O)$ photodetachment will preferentially dissociate to products, rather than reactants, even though both are energetically allowed. The vibrational levels of the HOHO complex have a somewhat different reactant/product character. Even though though the uncertainty of the OH+OH asymptote may energetically allow the $v'=1$ state of HOHO (peak *B*) to dissociate to reactants, the wave function in Fig. 13 shows that it most likely will be a product state. In contrast, the HOHO $v'=2$ wave function (peak *C*) is primarily a reactant wave function.

It is instructive to compare the results presented here to earlier studies[4] of the $OH+F\rightarrow O+HF$ and $CH_3OH+F\rightarrow CH_3O+HF$ reactions by photoelectron spectroscopy of

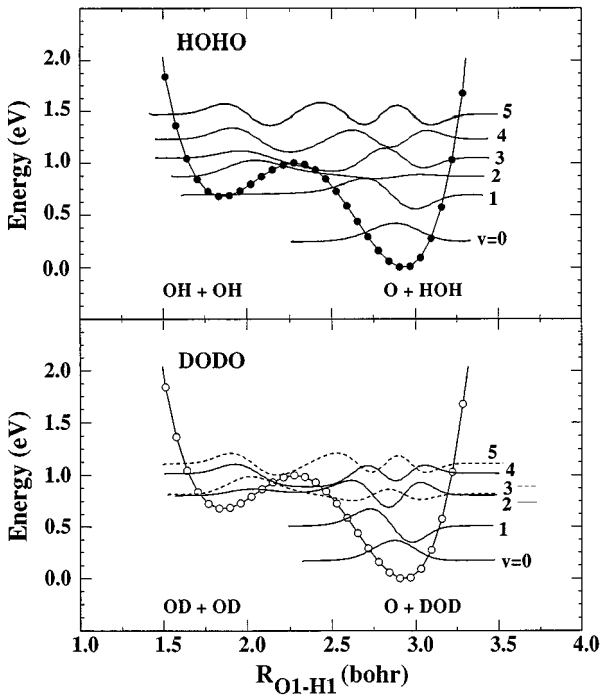

FIG. 13. The MP2/6-31++G** and QCISD/6-31++G** neutral potential energy curves or the HOHO complex (as in Fig. 8) with the associated eigenfunctions and eigenvalues.

Downloaded¬03¬Mar¬2003¬to¬128.32.220.150. Redistribution¬subject¬to¬AIP¬license¬or¬copyright,¬see¬http://ojps.aip.org/jcpo/jcpcr.jsp

OHF^- and CH_3OHF^-. In these earlier studies, there were also two channels for dissociation of the neutral complex (i.e., HF+O, OH+F), but the energetic separation was considerably larger: almost 1.5 eV vs 0.4 eV for the HOHO complex. Moreover, the one-dimensional potentials for vibrational motion of the central H atom are more asymmetric for OHF^- and CH_3OHF^- than for $O^-(H_2O)$, and the amplitude of the central H-atom motion in the ground vibrational state is therefore considerably smaller (almost half) for the F^- containing ions. Nonetheless, analysis of the OHF^- and CH_3OHF^- photoelectron spectra showed that photodetachment accesses states of the complex that correlate to reactants and products of the neutral reaction, just as in $O^-(H_2O)$ photodetachment.

This occurs because the OHF^- and CH_3OHF^- geometries are closer to the neutral transition state geometries than the corresponding anions for reactions (1) and (2). For example, *ab initio* calculations yield $R_e(HF)=1.35$ Å and $R_e(OH)=1.08$ Å for OHF^-, and $R(HF)=1.32$ Å and $R(OH)=1.08$ Å at the F+OH transition state;[4,68] these should be compared to the anion and transition state geometries in Figs. 5 and 9. Because the Franck–Condon region for OHF^- photodetachment is virtually centered on the neutral transition state, relatively little H-atom amplitude in the OHF^- ground state wave function is needed to overlap the reactant and product sides of the saddle point on the neutral potential energy surface. In contrast, the Franck–Condon regions for photodetachment of $O^-(H_2O)$ and $H_3O_2^-$ are centered at slightly larger O–O distance than their respective neutral transition states, but the larger H-atom amplitude in the anions still enables one to probe a relatively large region of the neutral potential energy surfaces.

C. Excited states

As mentioned above, both the $H_3O_2^-$ and the $O^-(H_2O)$ photoelectron spectra show evidence for photodetachment transitions to excited states of the neutral complex. The features which are assigned as excited states occur at eKEs which are significantly affected by the electron detector cutoff function. In fact, these features most likely represent only thresholds for excited states. Experiments at higher photon energies are necessary to determine the true characteristics of these features. As a result, little can be determined from this data about the nature of the excited state surfaces.

As mentioned above, several electronic states result from the interaction of two hydroxyl radicals. We have observed the $^3A''$ state and the $^3A'$ is not accessible by one-electron photodetachment. It is likely that the excited state represents photodetachment to form one of the singlet electronic states that exist. The 26 kcal/mole endothermicity[24] of the $OH+OH \rightarrow H_2O+O(^1D)$ places the lower limit for the asymptote at eKE=0.225 eV. It is quite possible that the feature at eKE=0.38 eV in the $O^-(H_2O)$ [0.30 eV in the $O^-(D_2O)$ spectrum] represents the onset of photodetachment to that surface. Fueno calculates the barrier for the neutral reaction to be 35 kcal/mole.[23]

While there are several possible electronic states which arise from the interaction of two OH radicals, there are a limited number of states available in the $OH+H_2O$ interaction. As mentioned above, we find that the $^2A''$ state of the HOHOH lies 0.58 eV above the $^2A'$ state at the anion geometry at the MP2/6-31++G** level of theory. This compares with the >1.1 eV spacing between peaks *A* and *D* in the $H_3O_2^-$ spectrum. It is unlikely that species correlating to electronically excited products will be observed because the first excited states of OH and H_2O lie are more than 4 eV above their respective ground states. Further experiments at higher photodetachment energies are required to identify the transitions which are responsible for these features.

V. SUMMARY

Negative ion photoelectron spectroscopy of $H_3O_2^-$ and $O^-(H_2O)$ has been used to study the transition state regions of the $OH+H_2O \rightarrow H_2O+OH$ and $OH+OH \rightarrow O(^3P)+H_2O$ hydroxyl radical reactions. In both cases, the several broad features, all of which are located above the energetic neutral dissociation asymptote, are assigned to vibrational motions of the unstable neutral complex perpendicular to the reaction coordinate, specifically the H-atom antisymmetric stretch. Calculated anion equilibrium geometries and the neutral transition state geometries suggest that the neutral complex studied in each experiments is near the transition state region for its respective reaction.

One-dimensional Franck–Condon analyses are performed using *ab initio* calculated H-atom antisymmetric stretch potential energy curves. Overall, the agreement between the 1-D simulations and the observed peak positions and intensities in photoelectron spectra supports the assignment of the observed features to $O\cdots\overleftrightarrow{H}\cdots O$ motion of the unstable [HOHOH] and [HOHO] complexes. The simple 1-D model is able to reproduce the rather complicated isotope effects quite well. However, the peak widths in the experimental spectra are also of considerable interest as they are result from a combination of higher dimensional effects (such as unresolved bend progressions) and the dissociation dynamics of the neutral complex.

In order to extract more information on reactions (1) and (2) from our photoelectron spectra, it is necessary to construct higher-dimensional potential energy surfaces for these reactions and to simulate the spectra with quantum dynamics calculations using these surfaces. Given the considerable progress in performing scattering calculations on the somewhat simpler $OH+H_2$ reaction,[69–73] including exact simulations of the $OH^-\cdot H_2$ photoelectron spectrum,[74] it is certainly reasonable to expect that accurate, full-dimensional simulations of the spectra presented here should be feasible in the not too distant future. As the focus of experimental and theoretical reaction dynamics shifts from three atom $A+BC$ reactions to polyatomic systems, we expect the transition state spectroscopy experiments of the type described here to play a major role in understanding how additional degress of freedom affect the dynamics of these more complex reactions.

ACKNOWLEDGMENTS

This work is supported by the United States Air Force Office of Scientific Research under Contract No. F49620-94-1-0115.

Downloaded¬03¬Mar¬2003¬to¬128.32.220.150. Redistribution¬subject¬to¬AIP¬license¬or¬copyright,¬see¬http://ojps.aip.org/jcpo/jcpcr.jsp

[1] R. B. Metz, S. E. Bradforth, and D. M. Neumark, Adv. Chem. Phys. **91**, 1 (1992); D. M. Neumark, Accts. Chem. Res. **26**, 33 (1993).
[2] S. E. Bradforth, A. Weaver, D. W. Arnold, R. B. Metz, and D. M. Neumark, J. Chem. Phys. **92**, 7205 (1990); A. Weaver, R. B. Metz, S. E. Bradforth, and D. M. Neumark, J. Phys. Chem. **92**, 5558 (1988).
[3] R. B. Metz, A. Weaver, S. E. Bradforth, T. N. Kitsopoulos, and D. M. Neumark, J. Phys. Chem. **94**, 1377 (1990).
[4] S. E. Bradforth, D. W. Arnold, R. B. Metz, A. Weaver, and D. M. Neumark, J. Phys. Chem. **95**, 8066 (1991).
[5] S. E. Bradforth, D. W. Arnold, D. M. Neumark, and D. E. Manolopoulos, J. Chem. Phys. **99**, 6345 (1993); D. E. Manolopoulos, K. Stark, H.-J. Werner, D. W. Arnold, S. E. Bradforth, and D. M. Neumark, Science **262**, 1852 (1993).
[6] R. Atkinson, Chem. Rev. **86**, 69 (1986).
[7] World Meteorological Organization, *Global Ozone Research and Monitoring Project*—Report No. 16 (1985).
[8] J. A. Logan, M. J. Prather, S. F. Wofsy, and M. B. McElroy, J. Geophys. Res. **86**, 7210 (1981); D. Perner, U. Platt, M. Trainer, G. Hübler, J. Drummond, W. Junkermann, J. Rudolph, B. Schubert, A. Volz, D. H. Ehhalt, K. J. Rumpel, and G. Helas, J. Atmos. Chem. **5**, 185 (1987).
[9] H. Levy, II, Planet. Space. Sci. **20**, 919 (1972).
[10] J. Warnatz, in *Combustion Chemistry*, edited by W. C. Gardiner, Jr. (Springer-Verlag, New York, 1984).
[11] C. M. Rohlfing, L. C. Allen, C. M. Cook, and H. B. Schlegel, J. Chem. Phys. **78**, 2498 (1983).
[12] Represents the average of the two values (26.8 and 27.6 kcal/mole) determined in the following references, respectively: M. Meot-Ner and L. W. Sieck, J. Phys. Chem. **90**, 6687 (1986); G. J. C. Paul and P. Kebarle, *ibid*. **94**, 5184 (1990).
[13] P. A. Schultz. R. D. Mead, P. L. Jones, and W. C. Lineberger, J. Chem. Phys. **77**, 1153 (1982).
[14] K. S. Kim, H. S. Kim, J. H. Jang, H. S. Kim, B.-J. Mhin, Y. Xie, and H. F. Schaefer, III, J. Chem. Phys. **94**, 2057 (1991).
[15] Y. Xie and H. F. Schaefer, III, J. Chem. Phys. **98**, 8829 (1993).
[16] A. A. Nanayakkara, G. G. Balint-Kurti, and I. H. Williams, J. Phys. Chem. **96**, 3662 (1992).
[17] C. Lifshitz, J. Phys. Chem. **86**, 3634 (1982).
[18] C. R. Moylan, J. A. Dodd, C.-C. Han, and J. I. Brauman, J. Chem. Phys. **86**, 5350 (1987).
[19] A. A. Viggiano, R. A. Morris, C. A. Deakyne, F. Dale and J. F. Paulson, J. Phys. Chem. **94**, 8193 (1990).
[20] F. C. Fehsenfeld and E. E. Ferguson, J. Chem. Phys. **61**, 3181 (1974).
[21] J. D. Payzant, R. Yamdgani, and P. Kebarle, Can. J. Chem. **49**, 3308 (1971).
[22] D. M. Neumark, K. R. Lykke, T. Anderson, and W. C. Lineberger, Phys. Rev. A **32**, 1890 (1985).
[23] T. Fueno, in *Applied Quantum Chemistry*, edited by V. H. Smith, *et al*. (Reidel, New York, 1986), p. 33.
[24] L. B. Harding, J. Phys. Chem. **95**, 8653 (1991).
[25] L. B. Harding and A. F. Wagner, *Twenty-Second Symposium (International) on Combustion* (The Combustion Institute, 1988), p. 983.
[26] S. Golub and B. Steiner, J. Chem. Phys. **49**, 5191 (1968).
[27] K. Abu-Dari, K. N. Raymond, and D. P. Freyberg, J. Am. Chem. Soc. **101**, 3688 (1979); K. Abu-Dari, D. P. Freyberg, and K. N. Raymond, Inorg. Chem. **18**, 2427 (1979).
[28] K. H. Harmon, B. A. Southworth, and P. A. Mounts, J. Mol. Struct. **296**, 69 (1993).
[29] G. D. Greenblatt and C. J. Howard, J. Phys. Chem. **93**, 1035 (1989).
[30] U. K. Kläning, E. Larsen, and K. Sehested, J. Phys. Chem. **98**, 8946 (1994).
[31] F. P. Del Greco and F. Kaufman, Discuss. Faraday Soc. **33**, 128 (1962); F. Kaufman, Ann. Geophys. **20**, 106 (1964).
[32] G. Dixon-Lewis, W. E. Wilson, and A. A. Westenberg, J. Chem. Phys. **44**, 2877 (1966); A. A. Westenberg, and A. deHaas, *ibid*. **58**, 4066 (1973).
[33] J. E. Breen and G. P. Glass, J. Chem. Phys. **52**, 1082 (1970).
[34] A. McKenzie, M. F. R. Mulcahy, and J. R. Steven, J. Chem. Phys. **59**, 3244 (1973).
[35] M. A. A. Clyne and S. Down, J. Chem. Soc. Faraday Trans. **70**, 253 (1974).
[36] W. T. Rawlins and W. C. Gardiner, Jr., J. Chem. Phys. **60**, 4676 (1974).
[37] D. W. Trainor and C. W. von Rosenberg, Jr., J. Chem. Phys. **61**, 1010 (1974).
[38] J. Ernst, H. Gg. Wagner, and R. Zellner, Ber. Bunsenges. Phys. Chem. **81**, 1270 (1977).
[39] G. Wagner and R. Zellner, Ber. Bunsenges. Phys. Chem. **85**, 1122 (1981); R. Zellner, F. Ewig, R. Paschke, and G. Wagner, J. Phys. Chem. **92**, 4184 (1988).
[40] M. T. Woolridge, R. K. Hanson, and C. T. Bowman, Int. J. Chem. Kinet. **26**, 389 (1994).
[41] R. Zellner, J. Phys. Chem. **83**, 18 (1979).
[42] E. A. Albers, K. Hoyermann, H. Gg. Wagner, and J. Wolfrum, *Thirteenth Symposium (International) on Combustion* (The Combustion Institute, 1971), p. 81; J. W. Sutherland, P. M. Patterson, and R. B. Klemm, *Twenty-Third Symposium (International) on Combustion* (The Combustion Institute, 1990), p. 51; A. Lifshitz and J. V. Michael, *ibid*., p. 59.
[43] J. V. Michael, Prog. Energy Combust. Sci. **18**, 327 (1992).
[44] D. Vogt, Adv. Mass Spectrom. **5**, 222 (1971).
[45] J. F. Paulson and P. J. Gale, Adv. Mass Spectrom. A **7**, 263 (1978).
[46] M. P. Karnett and R. J. Cross, Chem. Phys. Lett. **82**, 277 (1981).
[47] J. M. Van Doren, S. E. Barlow, C. H. DePuy, and V. M. Bierbaum, Int. J. Mass Spectrom. Ion Proc. **109**, 305 (1991).
[48] D. F. Varley, D. J. Levandier, and J. M. Ferrar, J. Chem. Phys. **96**, 8806 (1992).
[49] M. A. Buntine, D. J. Lavrich, C. E. Dessent, M. G. Scaron, and M. A. Johnson, Chem. Phys. Lett. **216**, 471 (1993).
[50] P. F. Knewstubb and T. M. Sugden, Nature **196**, 1311 (1962).
[51] C. B. Cleveland and J. R. Wiesenfeld, J. Chem. Phys. **96**, 248 (1992); D. S. King, D. G. Sauder, and M. P. Casassa, J. Chem. Phys. **97**, 5919 (1992) and references therein.
[52] D. G. Sauder, J. C. Stephenson, D. S. King, and M. P. Casassa, J. Chem. Phys. **97**, 952 (1992).
[53] M. A. Johnson, M. L. Alexander, and W. C. Lineberger, Chem. Phys. Lett. **112**, 285 (1984).
[54] B. E. Knox and B. P. Burtt, J. Chem. Phys. **28**, 1256 (1958).
[55] F. C. Fehsenfeld and E. E. Ferguson, J. Chem. Phys. **61**, 3181 (1974).
[56] C. E. Melton, J. Phys. Chem. **76**, 22 (1972).
[57] W. C. Wiley and I. H. McLaren, Rev. Sci. Instrum. **26**, 1150 (1955).
[58] B. O. Roos, W. P. Kraemer, and G. H. F. Diercksen, Theoret. Chim. Acta **42**, 77 (1976); S. Ikuta, J. Comput. Chem. **5**, 374 (1984); Z. Latajka and S Scheiner, J. Mol. Struct. **234**, 373 (1991); G. V. Yukhnevich, E. G. Kokhanova, A. I. Pavlyuchko, and V. V. Volkov, J. Mol. Struct. **122**, 1 (1985).
[59] V. Spirko, W. P. Kraemer, and A. Cejchan, J. Mol. Spectrosc. **136**, 340 (1989).
[60] C. M. Roehl, J. T. Snodgrass, C. A. Deakyne, and M. T. Bowers, J. Chem. Phys. **94**, 6546 (1991).
[61] The energy separation is using the spin projected energies (PMP2). The unprojected values (UMP2) provides a separation of 0.36 eV.
[62] The singlet transition state is calculated to lie 32 kcal/mole higher in energy than the triplet transition state species at the MRDCI//SCF level of theory. See Refs. 23 and 24.
[63] G. Herzberg, *Molecular Spectra and Molecular Structure I. Spectra of Diatomic Molecules* (Krieger, Malabar, 1989).
[64] G. Herzberg, *Molecular Spectra and Molecular Structure III. Electronic Spectra and Electronic Structure of Polyatomic Molecules* (Krieger, Malabar, 1991).
[65] T. N. Kitsopoulos, I. M. Waller, J. G. Loeser, and D. M. Neumark, Chem. Phys. Lett. **159**, 300 (1989); Y. Zhao, C. C. Arnold, and D. M. Neumark, J. Chem. Soc. Faraday Trans. **89**, 1449 (1993).
[66] M. J. Davis, H. Koizumi, G. C. Schatz, S. E. Bradforth, and D. M. Neumark, J. Chem. Phys. (in press).
[67] D. O. Harris, G. G. Engerholm, and W. D. Gwinn, J. Chem. Phys. **43**, 1515 (1965).
[68] J. J. Sloan, D. G. Watson, J. M. Williamson, and J. S. Wright, J. Chem. Phys. **75**, 1190 (1981).
[69] D. C. Clary, J. Chem. Phys. **95**, 7298 (1991); **96**, 3656 (1992); G. Nyman and D. C. Clary, *ibid*. **99**, 7774 (1993).
[70] D. Wang and J. M. Bowman, J. Chem. Phys. **96**, 8906 (1992).
[71] U. Manthe, T. Seideman, and W. H. Miller, J. Chem. Phys. **99**, 10078 (1993).
[72] D. H. Zhang and J. Z. H. Zhang, J. Chem. Phys. **100**, 2697 (1994).
[73] D. Neuhauser, J. Chem. Phys. **100**, 9272 (1994).
[74] W. H. Thompson and W. H. Miller, J. Chem. Phys. **101**, 8620 (1994).

Downloaded¬03¬Mar¬2003¬to¬128.32.220.150. Redistribution¬subject¬to¬AIP¬license¬or¬copyright,¬see¬http://ojps.aip.org/jcpo/jcpcr.jsp